AGU PUBLICATIONS

JGR

Journal of Geophysical Research: Atmospheres

RESEARCH ARTICLE

10.1002/2013JD020420

Key Points:
- A new empirical decomposition extracts meaningful modes from hydroclimatic data
- The spectral separation of modes is cleaner than that achieved by EEMD
- A nonlinear trend of river flow could be linked to global warming

Correspondence to:
A. Antico,
aantico@santafe-conicet.gov.ar

Citation:
Antico, A., G. Schlotthauer, and M. E. Torres (2014), Analysis of hydroclimatic variability and trends using a novel empirical mode decomposition: Application to the Paraná River Basin, *J. Geophys. Res. Atmos.*, *119*, doi:10.1002/2013JD020420.

Received 24 JUN 2013
Accepted 30 DEC 2013
Accepted article online 5 JAN 2014

Analysis of hydroclimatic variability and trends using a novel empirical mode decomposition: Application to the Paraná River Basin

A. Antico[1,2], G. Schlotthauer[1,3], and M. E. Torres[1,2,3]

[1]National Scientific and Technical Research Council, Argentina, [2]Facultad de Ingeniería y Ciencias Hídricas, Universidad Nacional de Litoral, Santa Fe, Santa Fe, Argentina, [3]Laboratorio de Señales y Dinámicas no Lineales, Facultad de Ingeniería, Universidad Nacional de Entre Ríos, Oro Verde, Entre Ríos, Argentina

Abstract The current understanding of hydroclimatic processes is largely based on time series analysis of observations such as river discharge. Although records of these variables are often nonlinear and nonstationary, they have been commonly analyzed by classical methods designed for linear and/or stationary data. This study investigates the possibility of analyzing hydroclimatic time series using a novel data-driven method named Complete Ensemble Empirical Mode Decomposition with Adaptive Noise (CEEMDAN), which is suitable for nonlinear and nonstationary signals. CEEMDAN is here applied to a monthly mean discharge record (1904–2010) of the Paraná River (South America). The results obtained in this way are interpreted by comparing them with CEEMDAN decompositions of other records such as climate index time series. It is found that Paraná flow modes consist of (i) annual and intraannual oscillations reflecting the rainfall seasonality of different Paraná Basin sectors, and (ii) interannual to interdecadal changes linked to climate cycles like El Niño/Southern Oscillation, the North Atlantic Oscillation, and the Interdecadal Pacific Oscillation. A nonlinear trend of Paraná discharge is found and reveals a monotonic increase that could be attributed to global warming and anthropogenic land-cover changes. The spectral separation of modes obtained using CEEMDAN is cleaner than that achieved by the Ensemble Empirical Mode Decomposition technique. This makes it easier to interpret CEEMDAN results. Hence, CEEMDAN is proposed as a powerful method for extracting physically meaningful information from hydroclimatic data.

1. Introduction

Time series analysis of hydroclimatic observations provides direct information about hydrological changes and, therefore, plays a key role in understanding and managing water resources. In this analysis, an important goal is to decompose the original data into variability modes (i.e., quasiperiodic oscillations) and long-term trends. To achieve this objective, traditional methods designed under the hypothesis that time series are stationary and/or produced by linear systems (e.g., Fourier-based methods of spectral analysis and digital filtering) have been extensively used. However, since hydroclimatic records usually do not satisfy such requirements, the reliability of the results obtained with these techniques is often limited. Thus, an alternative approach would be to analyze these data using methods specifically designed for nonlinear and nonstationary time series.

A data-driven algorithmic method named Empirical Mode Decomposition (EMD) has been recently proposed to decompose nonlinear and nonstationary data in several variability modes that have to fullfill certain conditions [see *Huang et al.*, 1998]. This method is adaptive since it is based and derived from the data. That is, EMD does not require a predetermined basis such as the sinusoidal functions of Fourier analysis, or the mother wavelets (e.g., Morlet, Daubechies, or many others) in the time scale wavelet decomposition. Further, EMD serves as a dyadic filter bank and is a temporally local analysis [*Flandrin et al.*, 2004]. Despite these virtues, an important limitation of EMD is the so-called "mode mixing problem" that arises when a clean spectral separation of modes is not attained [*Huang and Wu*, 2008; *Schlotthauer et al.*, 2009]. In order to help to alleviate this inconvenience, the Ensemble EMD (EEMD) technique was proposed by *Wu and Huang* [2009]. Although EEMD already proved to be useful for analyzing geophysical data [e.g., *Huang and Wu*, 2008; *Wu et al.*, 2008, 2011], it also has some drawbacks that may limit the understanding of the results. For instance, the signal reconstructed by EEMD has a residual noise and the mode mixing problem

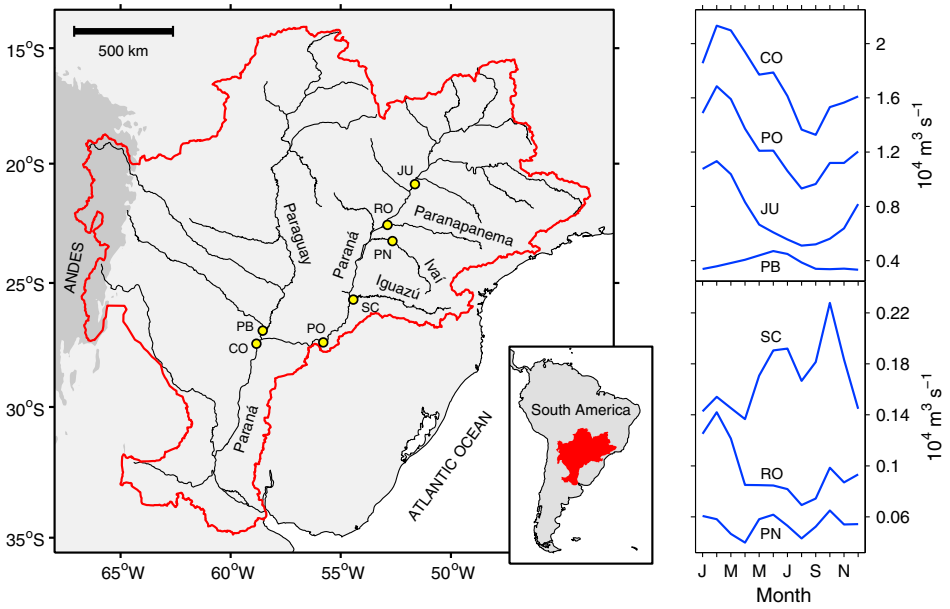

Figure 1. (left) Paraná River system (black lines) and its drainage basin (delimited by the red line); positions of gauging stations are indicated by open circles and the Andes Mountains (i.e., terrain with elevation greater than 2 km) are depicted by the dark grey region. (right) Climatological seasonal cycles of discharge measured at seven stations (flow data is described in Table 1); to facilitate the visualization of these cycles, offsets of +1000 and +200 $m^3 s^{-1}$ are added to the flows at stations JU and SC, respectively. River names mentioned in this paper are shown in left map. It must be noted that station CO is located south of the confluence of Paraguay and Paraná Rivers.

is still present in most applications to real data. These limitations motivated *Torres et al.* [2011] to develop a variant of the EEMD method, named Complete EEMD with Adaptive Noise (CEEMDAN), that yields an exact reconstruction of the original signal and a cleaner spectral separation of modes. Because of these strengths, CEEMDAN appears to be a powerful tool for extracting physically meaningful information from hydroclimatic time series, especially when the aforementioned problems are encountered. Up to our best knowledge, CEEMDAN had not yet been used to analyze this type of data.

The objective of this study is to investigate the potential usefulness of CEEMDAN for decomposing nonlinear and nonstationary hydroclimatic records into physically meaningful modes and trends. This goal is achieved by applying CEEMDAN to a record of monthly mean Paraná River discharge for the interval 1904–2010. Results from this decomposition are interpreted with the aid of CEEMDAN analysis of records that describe phenomena influencing the Paraná Basin hydroclimate (e.g., oscillations of the coupled atmosphere-ocean system). There is a considerable body of literature that explains how these phenomena affect the Paraná Basin, and thus provides a solid basis for the physical interpretation of our CEEMDAN results. For this reason, the Paraná River is chosen here as a case study.

In the following sections, we present the typical hydroclimatological conditions of the Paraná Basin (section 2), describe the hydroclimatic time series considered here and the methods used to analyze these data (sections 3 and 4), interpret the results obtained in this study (section 5), and give our main conclusions (section 6).

2. The Paraná River Basin

The Paraná Basin, with an area of about 2.6×10^6 km^2, is the second largest in South America and is located in the southeastern part of this continent between the Andes Mountains and the Atlantic Ocean (see Figure 1). As seen in Figure 2, the most intense precipitation falling over the Paraná Basin is associated with the summer occurrence of the South Atlantic Convergence Zone (SACZ) in the northeastern sector of this basin. In winter, the SACZ vanishes and rainfall is very low in this region (see Figure 2). Consequently, the seasonal flow variability of the middle and upper Paraná River is dominated by a large-amplitude annual cycle with high (low) discharge in summer (late winter and early spring) (see the climatological seasonal

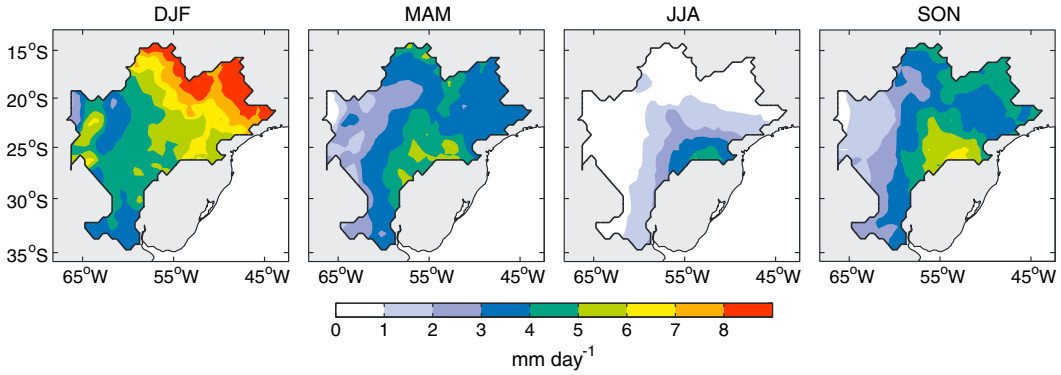

Figure 2. Seasonal climatological means of precipitation over the Paraná Basin. The following seasons are considered: December-January-February (DJF), March-April-May (MAM), June-July-August (JJA), and September-October-November (SON). Seasonal rainfall maps are constructed using the gridded (0.5° × 0.5°) climatology of the Global Precipitation Climatology Centre for the target interval 1951–2000 (version 2011) [*Meyer-Christoffer et al.*, 2011]. In the DJF map, orange and red regions depict intense rainfall associated with the South Atlantic Convergence Zone.

cycles of flow at Corrientes and Jupiá gauging stations in Figure 1) [*Camilloni and Barros*, 2000]. The SACZ also drives the annual cycle that dominates the flow seasonality of the Paraguay River, a Paraná tributary that drains a large part of the northern Paraná Basin. However, note from Figure 1 that the annual cycle of Paraguay discharge lags the annual cycle of Paraná flow by about 4 months. This delay is produced by the high water storage capacity of the Pantanal, a large wetland system located in the Paraguay Basin [*García and Vargas*, 1996; *Camilloni and Barros*, 2000]. Contrary to the Paraná and Paraguay Rivers, Paraná tributaries draining the east-central Paraná Basin do not exhibit a large-amplitude annual flow cycle. Figure 1 reveals that, in this region, tributaries such as the Iguazú, Ivaí, and Paranapanema Rivers are characterized by a small-amplitude 4 month cycle of discharge so that a local maximum (or inflection) is observed in summer, winter, and spring. While the summer maximum reflects a rainfall intensification associated with the SACZ, the remaining two maxima reflect precipitation enhancements due to the incursion of cold fronts, coming from the South Atlantic Ocean, in winter and spring [*García and Vargas*, 1996; *Camilloni and Barros*, 2000].

3. Data

Monthly mean discharges measured at gauging stations located along the Paraná River and along four Paraná tributaries are considered here (flow data are described in Table 1). These observed discharges may contain variations due to direct human activities (e.g., damming and deforestation). Note from Table 1 that there are few or no missing values in the discharge time series used here. Further, we have verified that the longest time interval of consecutive missing values spans only 4 months. Since these gaps of missing data are short, they are filled by using linear interpolation. Hereafter, the record of monthly mean discharge at station SN is denoted by Q_{SN} (symbols adopted here for gauging stations are given in Table 1).

Table 1. Records of Monthly Mean Discharge at Gauging Stations Located in the Paraná Basin

Station	Symbol	River	Time Span[a]	Missing Values[b]	Data Provider[c]
Corrientes	CO	Paraná	01/1904–12/2010	0	SSRH
Jupiá	JU	Paraná	07/1963–11/1985	13	GRDC
Paraíso do Norte	PN	Ivaí	04/1953–12/1996	2	NCAR
Posadas	PO	Paraná	01/1901–09/2000	0	SSRH
Puerto Bermejo	PB	Paraguay	09/1910–08/1994	8	SSRH
Rosana	RO	Paranapanema	01/1931–08/1975	0	NCAR
Salto Cataratas	SC	Iguazú	04/1942–12/1998	7	NCAR

[a]End and start times are given in month/year format.
[b]Total number of missing discharge values.
[c]GRDC: Global Runoff Data Centre (http://www.bafg.de/GRDC/); NCAR: National Center for Atmospheric Research (http://ncar.ucar.edu/); SSRH: Subsecretaría de Recursos Hídricos, Argentina (http://www.hidricosargentina.gov.ar/).

Table 2. Time Series of Climate Oscillation Indexes

Index	Symbol	Time Span[a]	Reference	Data Provider[b]
El Niño 3.4 index	N3.4	01/1871–12/2011	*Rayner et al.* [2003]	WGSP
Interdecadal Pacific Oscillation index	IPO	01/1871–12/2007	*Parker et al.* [2007]	C20C
Multivariate El Niño/Southern Oscillation index	MEI	01/1871–12/2005	*Wolter and Timlin* [2011]	ESRL
North Atlantic Oscillation index (PC-based)	NAO_{PC}	01/1899–12/2011	*Hurrell and Deser* [2009]	NCAR
North Atlantic Oscillation index (station-based)	NAO_{STN}	01/1900–12/2010	*Hurrell and Deser* [2009]	NCAR
Southern Oscillation index	SOI	01/1866–12/2011	*Ropelewski and Jones* [1987]	CRU

[a]End and start times are given in month/year format.
[b]C20C: Climate of the 20th century project (http://www.iges.org/c20c/); CRU: Climate Research Unit (http://www.cru.uea.ac.uk/); ESRL: Earth System Research Laboratory (http://www.esrl.noaa.gov/); NCAR: National Center for Atmospheric Research (http://ncar.ucar.edu/); WGSP: Working Group on Surface Pressure (http://www.esrl.noaa.gov/psd/gcos_wgsp/).

As shown in Figure 1, the flow at Corrientes station reflects precipitation integrated over most of the Paraná Basin. Thus, the discharge recorded at Corrientes is similar to that observed downstream of this station [*Camilloni and Barros*, 2000]. For this reason, the results obtained in this work using flow data from Corrientes station also serve to characterize discharge changes in the lowest stretch of the Paraná River.

Time series of climate oscillation indexes, used in the interpretation of Paraná flow changes, are described in Table 2. It is noted that these series are continuous (i.e., without missing values). Definitions of climate indexes are briefly presented below in this section (detailed definitions can be found in the references included in Table 2).

El Niño (EN) and La Niña (LN) events are opposite phases of El Niño/Southern Oscillation (ENSO), which is a cycle of the tropical Pacific climate with periods between 2 and 7 years [*Trenberth et al.*, 2007]. The following indexes are commonly used to characterize the time evolution of ENSO: (i) Niño 3.4 index (N3.4), which is the sea surface temperature (SST) averaged over the region bounded by 120°W–170°W and 5°S–5°N, and (ii) Southern Oscillation index (SOI), which is the normalized sea level pressure (SLP) difference between Tahiti and Darwin, Australia. Additionally, *Wolter and Timlin* [2011] calculated the multivariate ENSO index (MEI) by combining SLP and SST data. Whereas positive (negative) values of MEI and N3.4 correspond to EN (LN) events, negative (positive) values of SOI are associated with EN (LN) episodes. In order to facilitate the comparison of different ENSO indexes, the sign of the original SOI values is reversed in this study.

The North Atlantic Oscillation (NAO) is an interannual and interdecadal cycle of the North Atlantic climate. The time variability of the NAO is usually described by a station-based index that is calculated as the normalized SLP difference between Lisbon, Portugal, and Stykkisholmur/Reykjavik, Iceland [*Hurrell and Deser*, 2009]. An alternative version of this index is defined as the leading principal component (PC) of North Atlantic SLP [*Hurrell and Deser*, 2009].

At interdecadal time scales, a long-lasting ENSO-like pattern of climate variability was detected in the Pacific Ocean [*Trenberth et al.*, 2007]. This phenomenon is known as the Pacific Decadal Oscillation (PDO) when SST of the North Pacific Ocean is used to detect it and is named as the Interdecadal Pacific Oscillation (IPO) when SST of the whole basin is considered. Accordingly, the PDO index is defined as the leading PC of North Pacific SST [*Mantua et al.*, 1997], and the IPO index is defined as the second low-frequency PC of global SST [*Parker et al.*, 2007]. These two indexes have positive (negative) values for EN-like (LN-like) patterns and exhibit similar long-term variabilities [*Folland et al.*, 2002]. Nonetheless, as in previous studies regarding links between the Pacific Ocean and the hydroclimate of Australasia [e.g., *McKerchar and Henderson*, 2003; *Pui et al.*, 2011], we only consider the IPO index. This is because, like Australasian climate, South American climate can be affected by South Pacific SST changes that are included in the IPO-index definition but are excluded from the PDO-index definition.

In addition to the climate index records described above, continuous time series of the following variables are also used in the interpretation of Paraná flow variations: (i) global mean monthly mean surface

temperature anomalies (relative to 1961–1990) provided by the Climate Research Unit (CRU) and Met Office Hadley Centre for the interval 1850–2012 (version 4.2.0.0) [*Morice et al.*, 2012], and (ii) precipitation integrated over the Paraná Basin sector influenced by the SACZ. To calculate the latter, monthly gridded ($0.5° \times 0.5°$) reconstructions of land precipitation obtained from the CRU (version 3.10.01) [*Harris et al.*, 2013] and from the Global Precipitation Climatology Centre (GPCC) (full data reanalysis version 6) [*Schneider et al.*, 2011] are integrated north of 25°S and east of 60°W in the Paraná watershed (these integrals are denoted by P_{CRU} and P_{GPCC}, respectively). The Paraná Basin boundary of *Global Runoff Data Centre* [2007] is used to estimate P_{CRU} and P_{GPCC}. Time series of P_{CRU} and P_{GPCC} considered here span the intervals 1904–2009 and 1904–2010, respectively.

4. Methods

Methods used in this study to analyze hydroclimatic data are described in this section. Definitions of variability and trend adopted here are also given below.

4.1. Ensemble EMD

A detailed description of the EMD technique can be found in *Huang et al.* [1998]. This method is an iterative sifting process that decomposes a signal x (e.g., river flow record) into a number of oscillatory modes called Intrinsic Mode Functions (IMFs). *Huang et al.* [1998] define an IMF as a signal that satisfies two conditions: (i) the number of extrema and the number of zero crossings must be either equal or differ at most by one, and (ii) the mean value of the upper and lower envelopes is zero at any point. In the EEMD method, which is an improved version of EMD, definitive modes are defined as the average of the IMFs obtained through EMD over an ensemble of trials x^i ($i = 1, \dots, I$), generated by adding different white noise realizations w^i to the original signal x. More precisely, *Wu and Huang* [2009] described the EEMD algorithm as follows: (1) generate $x^i = x + \beta w^i$, where w^i ($i = 1, \dots, I$) is a zero-mean unit-variance white Gaussian noise, and β the level of added noise; (2) use EMD to fully decompose each x^i ($i = 1, \dots, I$) into the modes IMF_k^i, where $k = 1, \dots, K$ indicates the mode number; and (3) assign $\overline{\mathrm{IMF}}_k$ as the kth mode of x, obtained as the average of the corresponding IMFs: $\overline{\mathrm{IMF}}_k = \frac{1}{I}\sum_{i=1}^{I} \mathrm{IMF}_k^i$.

Note that $\overline{\mathrm{IMF}}_k$ does not necessarily satisfy the conditions required to be an IMF.

4.2. Complete EEMD With Adaptive Noise

Observe that in EEMD, each x^i is decomposed independently from the other realizations. Thus, different residues $r_k^i = r_{k-1}^i - \mathrm{IMF}_k^i$ ($r_0^i = x^i$) are obtained for different realizations. In CEEMDAN, the definitive kth mode is notated as $\widetilde{\mathrm{IMF}}_k$ and a single first residue is obtained as $r_1 = x - \widetilde{\mathrm{IMF}}_1$, with $\widetilde{\mathrm{IMF}}_1$ being the first EEMD mode [*Torres et al.*, 2011; *Colominas et al.*, 2012]. Then, the first EMD mode is computed over an ensemble of r_1 plus different realizations of a given noise, and $\widetilde{\mathrm{IMF}}_2$ is obtained by averaging. The procedure continues with the rest of modes until a stopping criterion is attained.

Defining the operator $E_j(\cdot)$, which gives the jth mode obtained by EMD, and the zero-mean unit-variance white Gaussian noise w^i, the CEEMDAN algorithm can be described as follows: (1) obtain the first EMD mode of I realizations $x + \beta_0 w^i$ ($i = 1, \dots, I$) and compute

$$\widetilde{\mathrm{IMF}}_1 = \frac{1}{I}\sum_{i=1}^{I} \mathrm{IMF}_1^i = \overline{\mathrm{IMF}}_1, \tag{1}$$

(2) calculate the first residue as: $r_1 = x - \widetilde{\mathrm{IMF}}_1$, (3) find the first EMD mode for each realization $r_1^i = r_1 + \beta_1 E_1(w^i)$ ($i = 1, \dots, I$) and define the second mode as:

$$\widetilde{\mathrm{IMF}}_2 = \frac{1}{I}\sum_{i=1}^{I} E_1\left(r_1 + \beta_1 E_1(w^i)\right), \tag{2}$$

(4) for $k = 2, \dots, K$ calculate the kth residue as:

$$r_k = r_{(k-1)} - \widetilde{\mathrm{IMF}}_k, \tag{3}$$

(5) compute the first EMD mode of $r_k + \beta_k E_k(w^i)$ $(i = 1, \ldots, I)$ and define the $(k+1)$th mode of CEEMDAN as:

$$\widetilde{\mathrm{IMF}}_{(k+1)} = \frac{1}{I}\sum_{i=1}^{I} E_1(r_k + \beta_k E_k(w^i)), \tag{4}$$

and (6) go to step 4 for next k.

Steps 4 to 6 are performed until the obtained residue can no longer be decomposed (i.e., the residue does not have at least two extrema). The final residue satisfies the following:

$$R = x - \sum_{k=1}^{K} \widetilde{\mathrm{IMF}}_k, \tag{5}$$

with K being the total number of modes. The signal x can be written as follows:

$$x = \sum_{k=1}^{K} \widetilde{\mathrm{IMF}}_k + R. \tag{6}$$

According to equation (6), the CEEMDAN decomposition is complete and allows an exact reconstruction of the original signal.

In CEEMDAN, the level of added noise is determined by the parameter β_k. Although different values of β_k can be set for different modes (see equation (4)), we use a fixed value of this parameter to obtain all modes. *Colominas et al.* [2012] found that, for CEEMDAN and EEMD, the added noise level and number of realizations can be adjusted depending on the application. In the present work, we set a noise level of 0.03, $I = 900$ realizations, and a maximum of 1000 sifting iterations in the CEEMDAN applications to time series of global surface temperature, IPO, N3.4, $\mathrm{NAO}_{\mathrm{STN}}$, P_{GPCC}, and SOI. For the rest of the records, the same parameter values are considered with the exception that the noise level is set to 0.3.

The implementations of CEEMDAN and EEMD used in this study are available at http://perso.ens-lyon.fr/patrick.flandrin/ and at http://www.bioingenieria.edu.ar/grupos/ldnlys/.

4.3. Definitions of Variability and Trend

We closely follow the EMD-based definitions of variability and trend proposed by *Wu et al.* [2007] for nonlinear and nonstationary data. Here the variability is defined as the set of CEEMDAN modes with oscillatory periods less than 90 years; for each mode, the characteristic oscillatory period (T) is estimated as the frequency corresponding to the most prominent peak of the raw periodogram. The trend is then obtained by subtracting all variability modes (i.e., all modes with $T < 90$ years) from the original data. Note that the trend extracted in this manner is adaptive and intrinsic since it is based on and derived from the raw data without the need of extrinsic and subjective functions (e.g., linear and exponential functions used in data fitting). When the physical mechanisms that generate the data are fully understood, an extrinsic approach for determining a trend could be a good choice. However, the understanding of processes that produce hydroclimatic data is usually incomplete and, therefore, an adaptive and data-driven approach would be more appropriate.

5. Results and Discussion

In this section, results obtained by applying CEEMDAN to the Paraná flow record from Corrientes station are (i) described separately for variability and trend (according to the definitions given in section 4.3) and (ii) physically interpreted with the help of decompositions of other hydroclimatic data. To do the latter, we used data describing hydroclimatic processes that are well known to affect the hydrological cycle of the Paraná Basin [*Garreaud et al.*, 2009]. The variability is depicted below by modes or sums of modes that are presented in ascending order of their oscillatory period, which is defined in section 4.3. Decompositions of Paraná flow achieved by CEEMDAN and EEMD are compared at the end of this section. Except for this EEMD decomposition, all results shown below are obtained using CEEMDAN.

Let us notice here that in what follows and for the sake of comparison with previous studies applying EMD and EEMD to geophysical data [e.g., *Huang and Wu*, 2008; *Wu et al.*, 2007, 2011], we will also refer to the

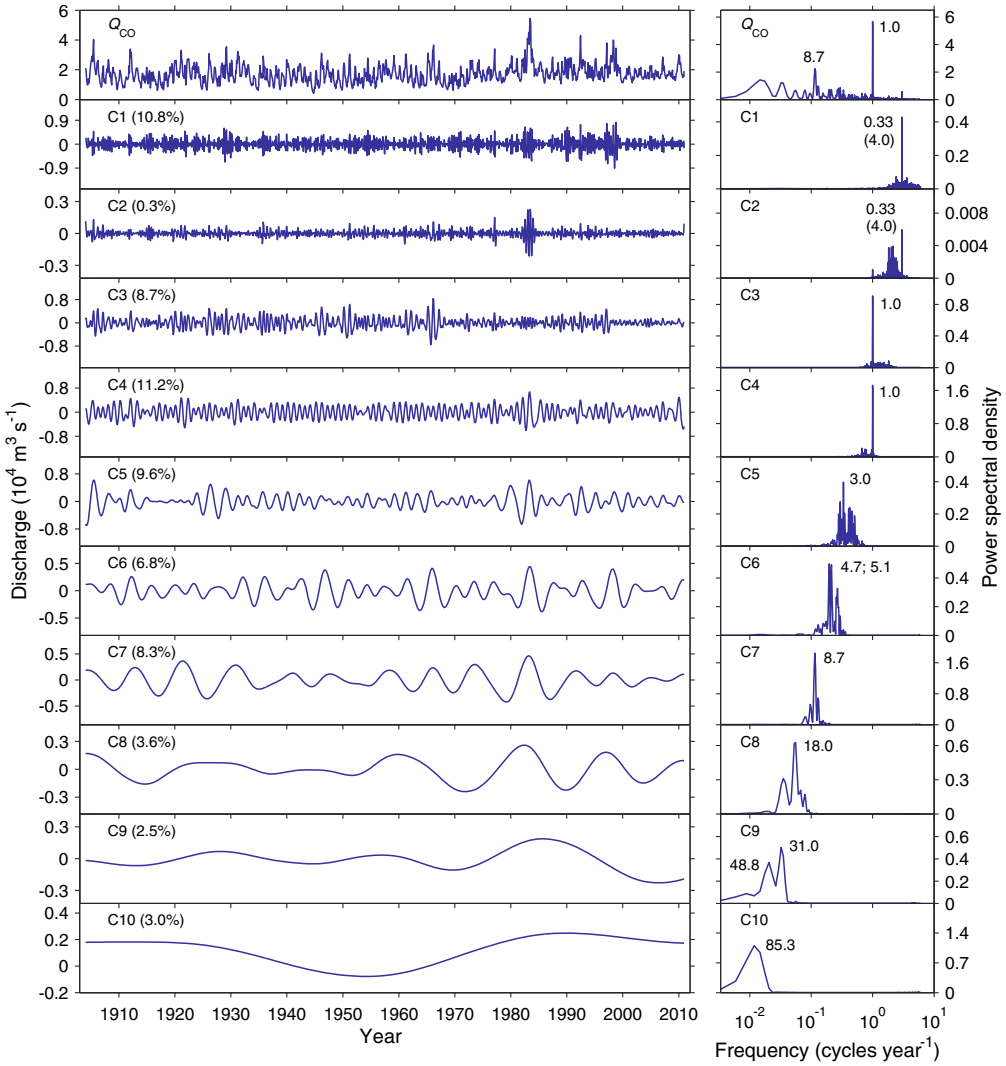

Figure 3. (left) Time series of Paraná discharge at Corrientes gauging station (Q_{CO}) and components of Q_{CO} extracted by CEEMDAN. (right) Raw periodograms of the Q_{CO} record and its components. In left, the fraction of total variance accounted by each component is shown within parentheses. In right, periods of the most prominent spectral peaks are given in years; for the intraannual components, these oscillatory periods are also given in months (within parenthesis).

CEEMDAN or EEMD modes as components. Hereafter, the *i*th mode extracted from a time series *x* is notated as C*i*(*x*).

5.1. Annual and Intraannual Variability ($T \leq 1$ Year)

In Figure 3, it can be observed that Paraná flow modes C1(Q_{CO}) and C2(Q_{CO}) oscillate with periods of about 4 months. This time scale also characterize the intraannual discharge variability of tributaries located in the east-central Paraná Basin (e.g., Iguazú, Ivaí, and Paranapanema Rivers) (see Figure 1). Indeed, as shown in Figure 4 and Table 3, discharge changes of C1(Q_{CO}) + C2(Q_{CO}) tend to follow those of C1($Q_{PN+RO+SC}$), where $Q_{PN+RO+SC}$ is the sum of Q_{PN}, Q_{RO}, and Q_{SC} (i.e., the sum of Ivaí, Parapanema, and Iguazú flows, respectively). Figure 4 and Table 3 also reveal a notable correspondence between C1(Q_{CO}) + C2(Q_{CO}) and C1(Q_{PO-JU}), where Q_{PO-JU} is the difference between Paraná flows at Posadas and Jupiá stations; note that Q_{PO-JU} integrates the precipitation falling over most of the east-central Paraná catchment (see Figure 1). Hence, C1(Q_{CO}) + C2(Q_{CO}) is interpreted as a 4 month Q_{CO} cycle originated in the east-central Paraná Basin, where a 4 month rainfall oscillation exists (see section 2). Table 3 indicates that the correlation between C1(Q_{CO}) + C2(Q_{CO}) and C1(Q_{PO-JU}) is significantly stronger than that between C1(Q_{CO}) + C2(Q_{CO}) and C1($Q_{PN+RO+SC}$). Probably, this is because while $Q_{PN+RO+SC}$ reflects the contribution of only three particular Paraná tributaries to the 4 month Q_{CO} cycle, Q_{PO-JU} includes the contribution of these and other tributaries.

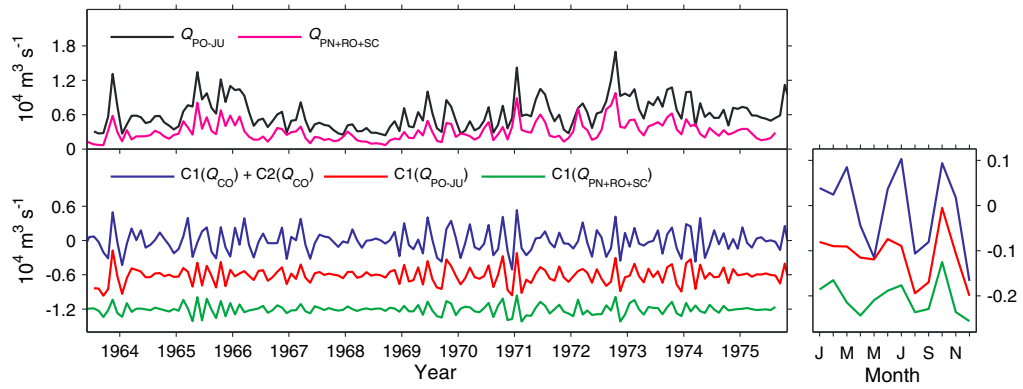

Figure 4. (top) Two estimates of the sum of tributary flows in the east-central Paraná Basin ($Q_{PN+RO+SC}$ and Q_{PO-JU}). (bottom left) Intraannual flow cycles captured by C1(Q_{CO}) + C2(Q_{CO}), C1($Q_{PN+RO+SC}$), and C1(Q_{PO-JU}). (bottom right) Climatological seasonal cycles of bottom left time series for the base interval July 1963 to August 1975 (flow in 10^4 m^3 s^{-1}). In bottom left, offsets of +1.2 and +0.6 are subtracted from the values of C1($Q_{PN+RO+SC}$) and C1(Q_{PO-JU}), respectively; in bottom right, offsets of +0.2 and +0.1 are subtracted from the values of C1($Q_{PN+RO+SC}$) and C1(Q_{PO-JU}), respectively.

As depicted in Figures 3 and 5, C3(Q_{CO}) + C4(Q_{CO}) is an annual cycle with high (low) discharges in summer (late winter and early spring). As mentioned in section 2, previous work revealed that this flow cycle is driven by the summer occurrence and winter disappearance of the SACZ in the northeastern Paraná Basin. This is confirmed by our results because, as seen in Figure 5 and Table 3, C3(Q_{CO}) + C4(Q_{CO}) is remarkably similar to the annual flow cycle captured by C3(Q_{JU}) + C4(Q_{JU}); note that Q_{JU} integrates rainfall only over the northeastern Paraná catchment (see location of station JU in Figure 1). Figure 5 and Table 3 also show that the correlation between C3(Q_{CO}) + C4(Q_{CO}) and C3(Q_{JU}) + C4(Q_{JU}) is slightly weaker than that between C3(Q_{CO}) + C4(Q_{CO}) and C3(Q_{JU+PB}) + C4(Q_{JU+PB}), where Q_{JU+PB} is the sum of Q_{JU} and Q_{PB} (i.e., the sum of upper Paraná and Paraguay flows, respectively). This is somehow expected because the Paraguay discharge has a SACZ-driven annual cycle that may contribute to the annual oscillation of Q_{CO} (see section 2). However, Table 3 shows that the difference between the aforementioned correlations is small and, consequently, the Paraguay River seems to play a minor role in the generation of C3(Q_{CO}) + C4(Q_{CO}).

5.2. Interannual Variability (1 Year < $T \leq$ 10 Year)

It can be seen from Figure 3 that the oscillatory periods of C5(Q_{CO}) and C6(Q_{CO}) are about 3 and 5 years, respectively, and coincide with characteristic ENSO periods. Moreover, as illustrated in Figure 6 and Table 3, typical ENSO cycles are positively correlated with C5(Q_{CO}) + C6(Q_{CO}) in such a way that discharge tends to be high (low) during El Niño (La Niña) events. Note that, although these correlations are moderate, they are statistically significant (see Table 3). Hence, our results are in agreement with previous studies where high and

Table 3. Zero-lag Pearson's correlation coefficient r_{xy} between the time series of variables x and y[a]

x	y	r_{xy}	Time span[b]
C1(Q_{CO}) + C2(Q_{CO})	C1($Q_{PN+RO+SC}$)	0.54(0.22)	07/1963–08/1975
C1(Q_{CO}) + C2(Q_{CO})	C1(Q_{PO-JU})	0.81(0.24)	07/1963–08/1975
C3(Q_{CO}) + C4(Q_{CO})	C3(Q_{JU}) + C4(Q_{JU})	0.78(0.43)	07/1963–11/1985
C3(Q_{CO}) + C4(Q_{CO})	C3(Q_{JU+PB}) + C4(Q_{JU+PB})	0.86(0.45)	07/1963–11/1985
C5(Q_{CO}) + C6(Q_{CO})	C5(MEI) + C6(MEI)	0.45(0.20)	01/1904–12/2005
C5(Q_{CO}) + C6(Q_{CO})	C4(N3.4) + C5(N3.4)	0.41(0.20)	01/1904–12/2010
C5(Q_{CO}) + C6(Q_{CO})	C4(SOI) + C5(SOI)	0.34(0.20)	01/1904–12/2010
C7(Q_{CO})	C7(NAO_{PC})	0.70(0.55)	01/1904–12/2010
C7(Q_{CO})	C6(NAO_{STN})	0.71(0.44)	01/1904–12/2010
C8(Q_{CO})	C8(P_{CRU})	0.75(0.58)	01/1904–12/2009
C8(Q_{CO})	C8(P_{GPCC})	0.73(0.63)	01/1904–12/2010
C9(Q_{CO}) + C10(Q_{CO})	C8(IPO) + C9(IPO) + C10(IPO)	0.88(0.68)	01/1904–12/2007

[a]Numbers within parenthesis indicate the 95% significance level for r_{xy}, which is estimated by combining 2000 Monte Carlo iterations with resampling in the frequency domain to consider autocorrelation [*Macias-Fauria et al.*, 2012]. Time spans considered in the calculation of r_{xy} are presented.

[b]End and start times are given in month/year format.

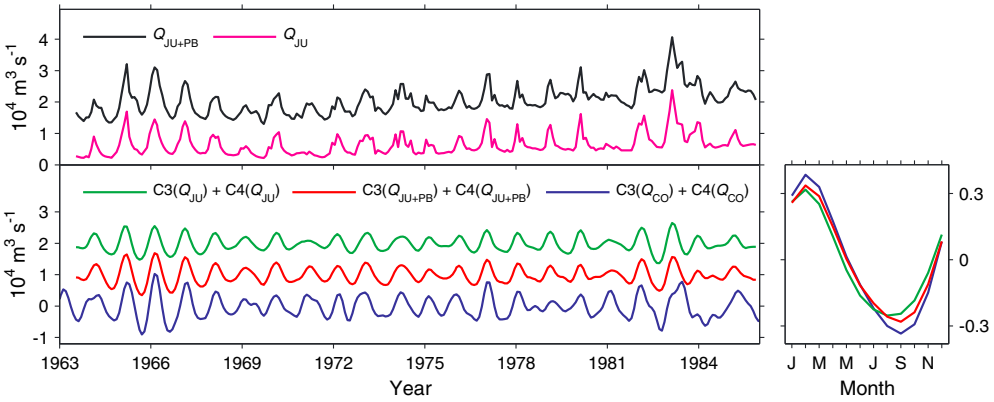

Figure 5. (top) Upper Paraná flow (Q_{JU}) and the sum of Upper Paraná and Paraguay discharges (Q_{JU+PB}); values of Q_{JU+PB} are increased by adding an offset of +1. (bottom left) Annual flow cycles diplayed by C3(Q_{CO}) + C4(Q_{CO}), C3(Q_{JU}) + C4(Q_{JU}), and C3(Q_{JU+PB}) + C4(Q_{JU+PB}); offsets of +2 and +1 are added to C3(Q_{JU}) + C4(Q_{JU}) and C3(Q_{JU+PB}) + C4(Q_{JU+PB}), respectively. (bottom right) Climatological seasonal cycles of bottom left time series for the base interval July 1963 to November 1985 (flow in 10^4 m^3 s^{-1}).

low Paraná flows have been related to El Niño and La Niña episodes, respectively [e.g., *Amarasekera et al.*, 1997; *Camilloni and Barros*, 2000, 2003; *Dettinger and Diaz*, 2000; *Grimm et al.*, 2000; *Robertson et al.*, 2001; *Berri et al.*, 2002; *Dai et al.*, 2009]. This ENSO-Paraná River link results from an intensification (weakening) of the subtropical jet stream during El Niño (La Niña) events that, in turn, increases (decreases) the baroclinic activity and associated rainfall over the Paraná Basin [see *Garreaud et al.*, 2009, and references therein].

Figure 3 reveals that C7(Q_{CO}) consists of an 8.7 year discharge cycle that was also detected in previous investigations of Paraná flow changes [e.g., *Robertson and Mechoso*, 1998; *Robertson et al.*, 2001; *Labat et al.*, 2005; *Pasquini and Depetris*, 2007; *Krepper et al.*, 2008; *Antico and Kröhling*, 2011]. Although the origin of this near-decadal cycle is not yet completely understood, previous observational studies have proposed a link with the NAO [*Robertson and Mechoso*, 1998; *Labat et al.*, 2005]. It has been suggested that, when the NAO index is positive (negative), an intensification (weakening) of the trade winds in the tropical North Atlantic Ocean enhances (diminishes) the moisture advection from this ocean to southeastern South America and this, in turn, increases (decreases) the Paraná flow. As evident from Figure 7 and Table 3, this NAO-Paraná River connection is supported by our results since maxima (minima) of C7(Q_{CO}) approximately coincide with maxima (minima) of near-decadal components of NAO-index records. Figure 7 also shows that there is a strong resemblance between the amplitude modulations of these Q_{CO} and NAO cycles. This further suggests the existence of a physical link between the NAO and the Paraná River.

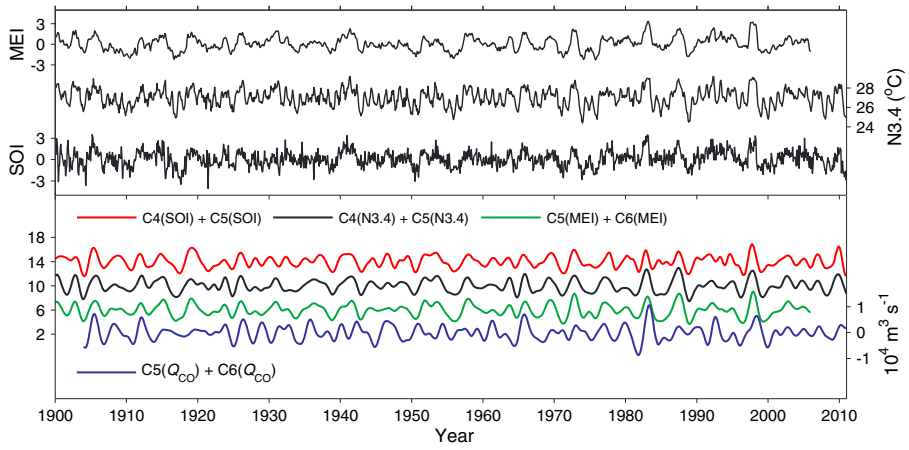

Figure 6. (top) Three indexes showing the ENSO state (MEI, N3.4, and SOI). (bottom) C5(Q_{CO}) + C6(Q_{CO}) (right vertical axis) and of 2–7 year cycles of ENSO indexes (left vertical axis); for each index, a filtered time series is obtained by adding the components with oscillatory periods between 2 and 7 years. Time series of C5(MEI) + C6(MEI), C4(N3.4) + C5(N3.4), and C4(SOI) + C5(SOI) are first divided by their respective standard deviations and then increased by adding offsets of +6, +10 and +14, respectively.

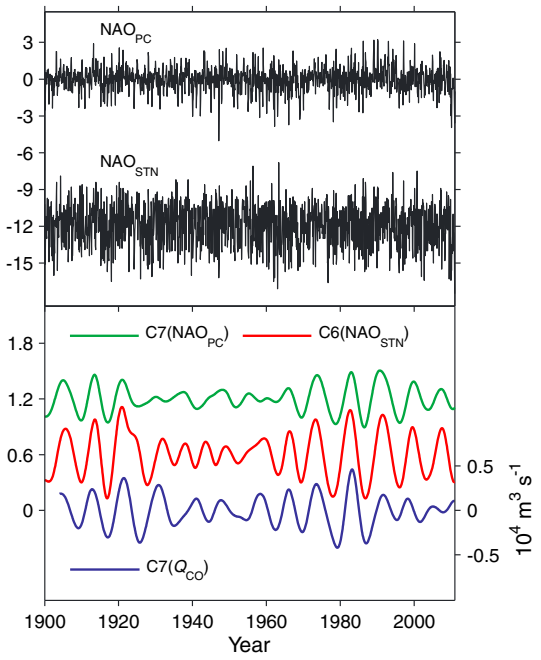

Figure 7. (top) Two versions of the NAO index (NAO_{PC} and NAO_{STN}); values of NAO_{STN} are reduced by subtracting an offset of +12. (bottom) C7(Q_{CO}) (right vertical axis) and NAO-index components with oscillatory periods of about 9 years (left vertical axis); offsets of +1.2 and +0.6 are added to C7(NAO_{PC}) and C6(NAO_{STN}), respectively.

5.3. Interdecadal Variability (10 Year < *T* < 90 Year)

Figure 3 indicates that C8(Q_{CO}) mainly oscillates with a period of 18 years. *Robertson et al.* [2001] found a similar 17 year cycle by analyzing summer-mean Paraná discharge data. *Robertson and Mechoso* [2000] discovered that this flow oscillation appears to be driven by interdecadal changes in the SACZ intensity, which are related to an anomalous upper-tropospheric large-scale eddy located in the lee side of the Andes Mountains. In agreement with this previous study, our Figure 8 and Table 3 show that flow variations in C8(Q_{CO}) follow changes in near-bidecadal components of SACZ-related rainfall.

Notoriously, although *Robertson et al.* [2001] found a 17 year cycle by performing a Singular Spectrum Analysis (SSA) on a summer-mean (January, February, and March) Paraná discharge record (1904–1997), *Robertson and Mechoso* [1998] did not detect a similar near-bidecadal cycle in their spectral analysis and SSA decomposition of an annual-mean Paraná flow record (1911–1993). Thus, according to *Wu et al.* [2008], this could be viewed as an example of different results derived from different time series that were obtained by averaging the same variable over different parts of the year. That is, the use of different definitions of interdecadal variability such as "interdecadal variability of annual means" and "interdecadal variability of summer means" for analyzing the same data set may lead to multiple results and interpretations. As stated by *Wu et al.* [2008], EMD and its recent variants (e.g., CEEMDAN) contribute to overcome this problem since these methods do not require a particular definition of interannual or interdecadal variability. In fact, our CEEMDAN decomposition of Paraná flow is able to extract an 18 year cycle directly from the raw monthly data (i.e., without considering annual or seasonal means).

As illustrated in Figure 3, the oscillatory periods of C9(Q_{CO}) and C10(Q_{CO}) are between 25 and 90 years. It can be observed from Figure 9 that discharge anomalies in C9(Q_{CO}) + C10(Q_{CO}) are only negative between 1939 and 1972 and this is consistent with the low-flow interval 1930–1970 detected in previous studies regarding flow tendency and channel morphology of the Paraná River [*García and Vargas*, 1998; *Amsler et al.*, 2005]. Moreover, flow anomalies in C9(Q_{CO}) + C10(Q_{CO}) are predominantly positive before 1939 and after 1972 (see Figure 9) and are concordant with the high-flow intervals 1904–1930 and 1970–1995 identified in these previous studies. As discussed immediately below, the occurrence of these high- and low-flow intervals appears to be related to the interdecadal Pacific variability.

Trenberth et al. [2007] noted that the Paraná discharge increased after the 1976–1977 abrupt change in the PDO index from negative to positive values, which is accompanied by a similar change in the IPO index. Our

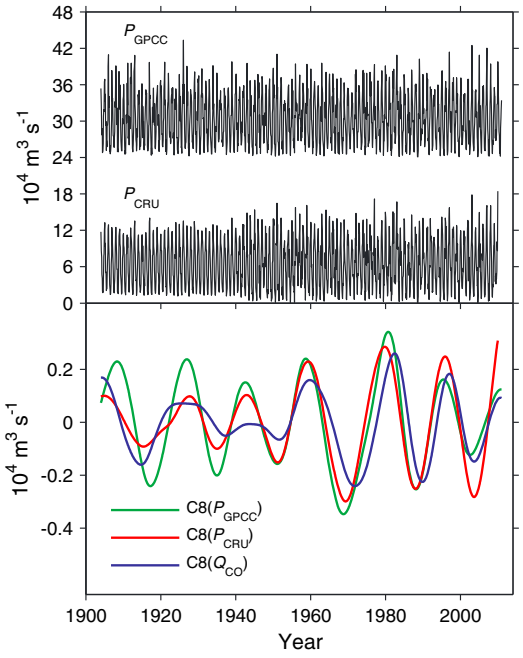

Figure 8. (top) Two estimates of the integral of rainfall over the Paraná Basin sector influenced by the SACZ (P_{CRU} and P_{GPCC}); values of P_{GPCC} are increased by adding an offset of +24. (bottom) C8(Q_{CO}) and components of integrated rainfall with oscillatory periods of about 18 years.

Figure 9 and Table 3 reveal that this type of IPO-Paraná River relationship is also present during the entire interval 1904–2010, when flow variations in C9(Q_{CO}) + C10(Q_{CO}) tend to follow changes in C8(IPO) + C9(IPO) + C10(IPO); the latter comprises all IPO-index components with oscillatory periods between 25 and 90 years. Figure 9 also shows that this concordance is remarkable after 1970, when the 25–90 year cycles of Q_{CO} and IPO index are approximately in phase. Before 1970, there are time lags of 4–6 years between these IPO and Q_{CO} oscillations (see Figure 9) that could be an artifact associated with large errors of the SST data corresponding to the first half of the 20th century. Notwithstanding these lags, the results presented here provide to the best of our knowledge the first empirical evidence for an IPO-Paraná River link during most of the

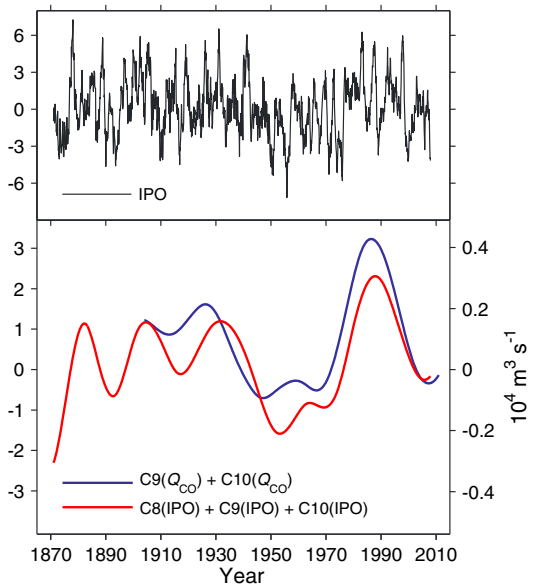

Figure 9. (top) Index showing the IPO state. (bottom) C9(Q_{CO}) + C10(Q_{CO}) (right vertical axis) and the sum of IPO-index components with oscillatory periods between 25 and 90 years (left vertical axis).

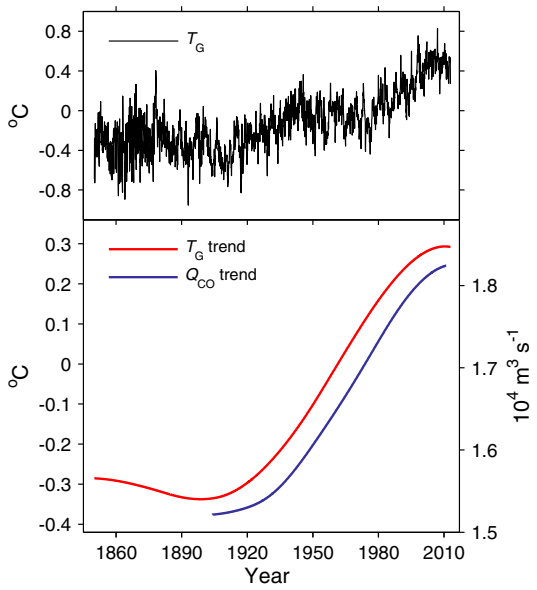

Figure 10. (top) Global-mean surface temperature anomalies relative to the interval 1961–1990 (T_G). (bottom) Nonlinear trends of Q_{CO} (right vertical axis) and of T_G (left vertical axis).

twentieth century and beginning of the 21st century. According to this evidence and to the ENSO-Paraná River connection discussed in section 5.2, the IPO-Paraná flow relationship found here is ENSO-like in the sense that river discharge tends to be larger during El Niño-like IPO years than in La Niña-like IPO years (as mentioned in section 3, the IPO is a long-lasting ENSO-like climate cycle). This is consistent with the results of *Garreaud et al.* [2009], who found that the spatial pattern of South American rainfall anomalies produced by ENSO cycles is similar to that associated with the ENSO-like Pacific interdecadal variability. Hence, it is possible that the physical mechanism underlying the ENSO-Paraná flow link (see section 5.2) also operates at IPO frequencies and, therefore, explains the observed IPO-Paraná River relationship.

5.4. Trend

Figure 10 shows that the obtained trend of Paraná discharge is nonlinear and exhibits a monotonic rise. Overall, this is in agreement with previous studies that also revealed upward trends of flow and precipitation in the Paraná Basin during most of the twentieth century and first decade of the 21st century [e.g., *Barros et al.*, 2000; *Pasquini and Depetris*, 2007; *Trenberth et al.*, 2007]. Similar increasing trends were detected in previous work but only during the second half of the twentieth century [*Genta et al.*, 1998; *Boulanger et al.*, 2005; *Pasquini and Depetris*, 2007; *Krepper et al.*, 2008; *Milliman et al.*, 2008; *Dai et al.*, 2009]. Note, however, that upward trends found in Paraná discharge records spanning 50 years or less would mainly reflect an increasing part of the 25–90 year flow cycles described in section 5.3.

At the global scale, both theoretical and modeling studies indicate that global warming is expected to produce an intensification of the water cycle, which would be manifested as increases in river discharge, evaporation, precipitation, and risk of extreme events (e.g., floods and droughts) [see *Trenberth et al.*, 2007, and references therein]; the theoretical basis for this intensification is rooted on the Clausius-Clapeyron relation which states that the saturated specific humidity increases approximately exponentially with temperature. At river basin scales, however, a streamflow trend can be upward or downward, depending on how global warming affects the balance between precipitation and evapotranspiration in the river basin. For the particular case of the Paraná River, our results shown in Figure 10 suggest that the effect of global warming is to increase flow since the trends of Paraná discharge and of global-mean surface temperature are upward and have strikingly similar shapes (the linear correlation coefficient between these trends is greater than 0.99). Such a global warming induced enhancement of flow would result from an increase in moisture advection from the Atlantic Ocean to the Paraná Basin. Interestingly, this mechanism is supported by the upward SST trends detected in the oceanic moisture source regions of the Paraná Basin (i.e., tropical Atlantic and subtropical South Atlantic oceans) [*Trenberth et al.*, 2007], given that sea surface evaporation increases with SST. Contrary to these SST changes, upward trends of land-surface air temperature detected

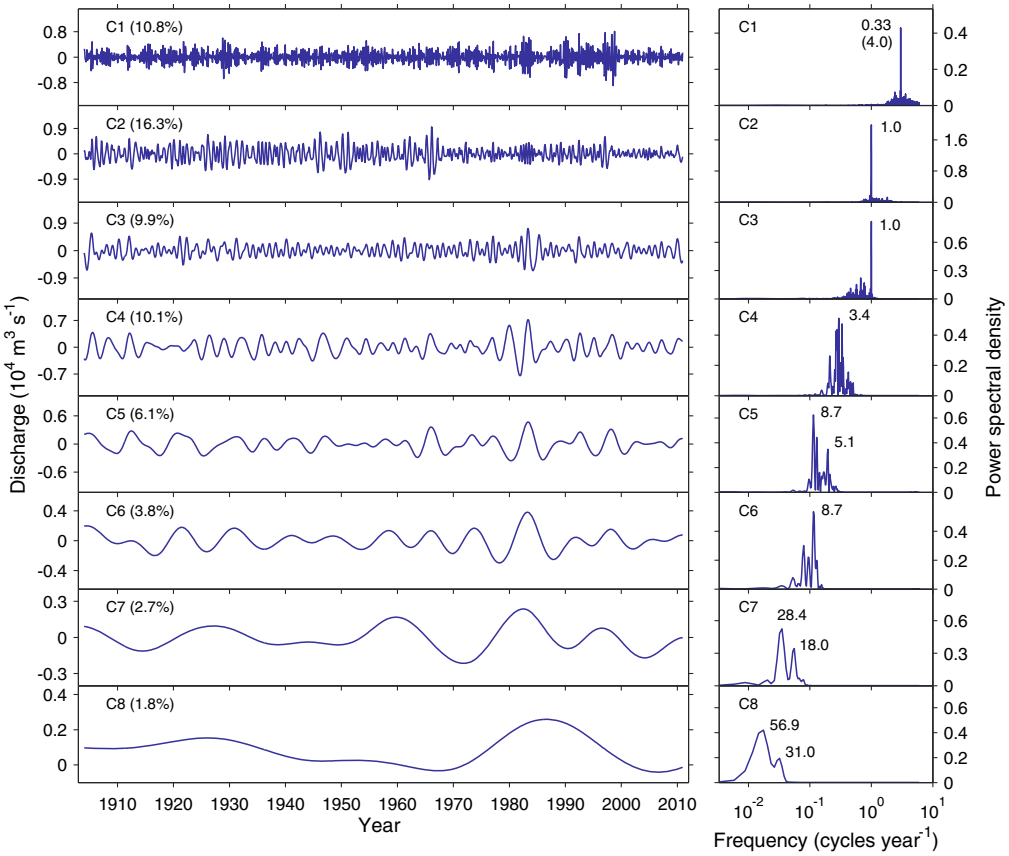

Figure 11. Same as Figure 3, but for the components of Q_{CO} obtained using EEMD. Note that the time series and power spectra of Q_{CO} are not shown.

in the Paraná catchment [*Trenberth et al.*, 2007] could have tended to decrease river flow by intensifying evapotranspiration. Nevertheless, the observed long-term increase in Paraná flow suggests that any possible intensification of evapotranspiration was overcompensated by an increase in precipitation.

Despite the above presented evidences for a contribution of global warming to the upward trend of Paraná discharge, it is worth noting that direct human influences (e.g., deforestation and land use changes) could also have contributed to increase flow [*Krepper et al.*, 2008; *Milliman et al.*, 2008, and references therein]. Although some of these influences have occurred throughout the entire twentieth century (e.g., deforestation), it is believed that the most important human alterations began in the 1970s (e.g., land changes associated with the introduction of intensive agriculture) [*Tucci and Clarke*, 1998; *Krepper et al.*, 2008]. Hence, it is likely that the direct anthropogenic contribution to the observed Paraná flow trend became important only since the 1970s.

An increase of the aerosol burden due to human activities (e.g., forest burning) has the potential to drive long-term changes in the global hydrological cycle [*Wu et al.*, 2013]. However, in the Paraná Basin, the possible contribution of anthropogenic aerosols to the observed hydrological trends still is uncertain [*Marengo et al.*, 2010].

5.5. Comparison of CEEMDAN and EEMD Results

CEEMDAN and EEMD decompositions of Paraná flow at Corrientes station are compared here. In order to ensure a consistent comparison, the parameter values selected for the CEEMDAN decomposition (see section 4.2) are also used in the EEMD implementation. Comparison of Figures 3 and 11 indicates that, contrary to CEEMDAN components, EEMD modes are not clearly separated from each other in the frequency domain, especially at interannual and interdecadal frequencies. For instance, as shown in Figure 11, the EEMD modes C5(Q_{CO}) and C6(Q_{CO}) are both dominated by 8.7 year cycles. Note also that a clean spectral separation of 18 year and 31 year flow cycles is achieved by CEEMDAN but not by EEMD (compare Figures 3

and 11). Therefore, our results suggest that CEEMDAN can provide a solution to the mode mixing problem when EEMD is not able to solve this inconvenience.

6. Conclusions

We have investigated the ability of a novel data-driven decomposition method to extract meaningful information from nonlinear and nonstationary hydroclimatic data. This method is a variant of the Ensemble Empirical Mode Decomposition (EEMD) technique and is named Complete EEMD with Adaptive Noise (CEEMDAN). A 107 year long time series of monthly Paraná River discharge has been analyzed using CEEMDAN. The main conclusions of this work are the following:

1. CEEMDAN succeeds in extracting 10 physically meaningful modes (i.e., cycles) from the Paraná flow record. Discharge modes with oscillatory periods equal and less than 1 year reflect the rainfall seasonality of different Paraná Basin sectors. The remaining modes of Paraná flow, which have lower frequencies, are related to climate oscillations (e.g., El Niño/Southern Oscillation and North Atlantic Oscillation). Although the climate-Paraná River links described here are in good overall agreement with those found in previous studies, our results additionally provide new insights into the Paraná flow variability. For example, we have found a novel evidence for a connection between the Paraná River and the Interdecadal Pacific Oscillation.
2. CEEMDAN-derived trends of Paraná flow and global-mean surface temperature are nonlinear, upward, and strikingly similar. This resemblance and theoretical considerations suggest that these trends are related to each other. Anthropogenic land-cover changes could also have contributed to the Paraná discharge trend, especially since the 1970s. Thus, CEEMDAN could significantly help to detect long-term hydrological changes due to global warming and direct anthropogenic activities. This is partly because, like EEMD, CEEMDAN allows the extraction of trends without the need of the assumptions and simplifications that are usually found in traditional techniques (e.g., the arbitrary choice of a linear or exponential function in a least squares minimum fit).
3. The spectral separation of Paraná discharge modes achieved by CEEMDAN is cleaner than that obtained using EEMD, especially at low frequencies. This facilitates the isolation and physical interpretation of flow cycles with different frequencies. Hence, CEEMDAN offers a solution to the mode mixing problem, particularly when EEMD fails in solving this inconvenience.

Finally, it should be stressed that, although the results presented here are very promising, more work should be done to further show the usefulness of CEEMDAN in studying hydroclimatic phenomena. For instance, since the Paraná Basin is taken here as a case study, it would be advisable to use CEEMDAN for studying the hydroclimatic variability of other regions. Furthermore, EEMD and its variants are pure empirical methods, and thus, there is a need to find a theoretical foundation that can explain the validity of empirical results [*Huang and Wu*, 2008]. Therefore, taking these considerations into account, we offer this study as a step forward in exploring the use of EEMD-based decomposition methods to analyze hydroclimatic data.

Acknowledgments
We are grateful to three anonymous reviewers for their constructive comments that improved the manuscript. This work was supported by the PIRHCa and PRODACT programs at the Facultad de Ingeniería y Ciencias Hídricas, Universidad Nacional de Litoral, Argentina.

References

Amarasekera, K. N., R. F. Lee, E. R. Williams, and E. A. B. Eltahir (1997), ENSO and the natural variability in the flow of tropical rivers, *J. Hydrol.*, *200*, 24–39.

Amsler, M. L., C. G. Ramonell, and H. A. Toniolo (2005), Morphologic changes in the Paraná River channel (Argentina) in the light of the climate variability during the 20th century, *Geomorphology*, *70*, 257–278, doi:10.1016/j.geomorph.2005.02.008.

Antico, A., and D. M. Kröhling (2011), Solar motion and discharge of Paraná River, South America: Evidence for a link, *Geophys. Res. Lett.*, *38*, L19401, doi:10.1029/2011GL048851.

Barros, V., M. E. Castañeda, and M. Doyle (2000), Recent precipitation trends in Southern South America East of the Andes: An indication of climatic variability, in *Southern Hemisphere Paleo- and Neoclimates*, edited by P. Smolka and W. Volkheimer, pp. 187–206, Springer, Berlin, Heidelberg.

Berri, G. J., M. A. Ghietto, and N. O. García (2002), The influence of ENSO in the flows of the upper Paraná River of South America over the past 100 years, *J. Hydromet.*, *3*, 57–65.

Boulanger, J. P., J. Leloup, O. Penalba, M. Rusticucci, F. Lafon, and W. Vargas (2005), Observed precipitation in the Paraná-Plata hydrological basin: Long-term trends, extreme conditions and ENSO teleconnections, *Clim. Dyn.*, *24*, 393–413, doi:10.1007/s00382-004-0514-x.

Camilloni, I. A., and V. R. Barros (2000), The Paraná River response to El Niño 1982–83 and 1997–98 events, *J. Hydromet.*, *1*, 412–430.

Camilloni, I. A., and V. R. Barros (2003), Extreme discharge events in the Paraná River and their climate forcing, *J. Hydrol.*, *278*, 94–106, doi:10.1016/S0022-1694(03)00133-1.

Colominas, M. A., G. Schlotthauer, M. E. Torres, and P. Flandrin (2012), Noise-assisted EMD methods in action, *Adv. Adapt. Data Anal.*, *4*, 11, doi:10.1142/S1793536912500252.

Dai, A., T. Qian, K. E. Trenberth, and J. D. Milliman (2009), Changes in continental freshwater discharge from 1948 to 2004, *J. Clim.*, *22*, 2773–2792, doi:10.1175/2008JCLI2592.1.

Dettinger, M. D., and H. F. Diaz (2000), Global characteristics of stream flow seasonality and variability, *J. Hydrometeor*, *1*, 289–310.

Flandrin, P., G. Rilling, and P. Gonçalvès (2004), Empirical mode decomposition as a filter bank, *IEEE Signal Process. Lett.*, *11*, 112–114, doi:10.1109/LSP.2003.821662.

Folland, C. K., J. A. Renwick, M. J. Salinger, and A. B. Mullan (2002), Relative influences of the interdecadal pacific oscillation and ENSO on the South Pacific convergence zone, *Geophys. Res. Lett.*, *29*, 1643, doi:10.1029/2001GL014201.

García, N. O., and W. M. Vargas (1996), The spatial variability of runoff and precipitation in the Rio de la Plata basin, *Hydrolog. Sci. J.*, *41*(3), 279–299.

García, N. O., and W. M. Vargas (1998), The temporal climatic variability in the 'Río de la Plata' basin displayed by the river discharges, *Clim. Change*, *38*, 359–379.

Garreaud, R. D., M. Vuille, R. Compagnucci, and J. Marengo (2009), Present-day South American climate, *Paleog. Paleoclim. Paleoecol.*, *281*, 180–195, doi:10.1016/j.palaeo.2007.10.032.

Genta, J., G. Perez-Iribarren, and C. R. Mechoso (1998), A recent increasing trend in the streamflow of rivers in southeastern South America, *J. Clim.*, *11*, 2858–2862.

Global Runoff Data Centre (2007), *Major River Basins of the World*, Global Runoff Data Centre, Federal Institute of Hydrology (BfG), Koblenz, Germany.

Grimm, A. M., V. R. Barros, and M. E. Doyle (2000), Climate variability in southern South America associated with El Niño and La Niña events, *J. Clim.*, *13*, 35–58.

Harris, I., P. Jones, T. Osborn, and D. Lister (2013), Updated high-resolution grids of monthly climatic observations—The CRU TS3.10 dataset, *Int. J. Climatol.*, doi:10.1002/joc.3711.

Huang, N., and Z. Wu (2008), A review on Hilbert-Huang transform: Method and its applications to geophysical studies, *Rev. Geophys.*, *46*, 8755–1209, doi:10.1029/2007RG000228.

Huang, N. E., Z. Shen, S. R. Long, M. C. Wu, H. H. Shih, Q. Zheng, N.-C. Yen, C. C. Tung, and H. H. Liu (1998), The empirical mode decomposition and the Hilbert spectrum for nonlinear and non-stationary time series analysis, *Proc. R. Soc. London, Ser. A*, *454*, 903–995.

Hurrell, J. W., and C. Deser (2009), North Atlantic climate variability: The role of the North Atlantic Oscillation, *J. Mar. Syst.*, *78*, 28–41, doi:10.1016/j.jmarsys.2008.11.026.

Krepper, C. M., N. O. García, and P. D. Jones (2008), Low-frequency response of the upper Paraná basin, *Int. J. Climatol.*, *28*, 351–360.

Labat, D., J. Ronchail, and J. L. Guyot (2005), Recent advances in wavelet analyses: Part 2-Amazon, Parana, Orinoco and Congo discharges time scale variability, *J. Hydrol.*, *314*, 289–311, doi:10.1016/j.jhydrol.2005.04.004.

Macias-Fauria, M., A. Grinsted, S. Helama, and J. Holopainen (2012), Persistence matters: Estimation of the statistical significance of paleoclimatic reconstruction statistics from autocorrelated time series, *Dendrochronologia*, *30*, 179–187, doi:10.1016/j.dendro.2011.08.003.

Mantua, N. J., S. R. Hare, Y. Zhang, J. M. Wallace, and R. C. Francis (1997), A Pacific interdecadal climate oscillation with impacts on salmon production, *Bull. Am. Meteorol. Soc.*, *78*, 1069–1079.

Marengo, J. A., et al. (2010), Recent developments on the South American monsoon system, *Int. J. Climatol.*, *32*, 1–2, doi:10.1002/joc.2254.

McKerchar, A. I., and R. D. Henderson (2003), Shifts in flood and low-flow regimes in New Zealand due to interdecadal climate variations, *Hydrolog. Sci. J.*, *48*, 637–654, doi:10.1623/hysj.48.4.637.51412.

Meyer-Christoffer, A., A. Becker, P. Finger, B. Rudolf, U. Schneider, and M. Ziese (2011), GPCC climatology version 2011 at 0.5°: Monthly land-surface precipitation climatology for every month and the total year from rain-gauges built on GTS-based and historic data, doi:10.5676/DWD_GPCC/CLIM_M_V2011_050.

Milliman, J. D., K. L. Farnsworth, P. D. Jones, K. H. Xu, and L. C. Smith (2008), Climatic and anthropogenic factors affecting river discharge to the global ocean, 1951–2000, *Global Planet. Change*, *62*, 187–194, doi:10.1016/j.gloplacha.2008.03.001.

Morice, C. P., J. J. Kennedy, N. A. Rayner, and P. D. Jones (2012), Quantifying uncertainties in global and regional temperature change using an ensemble of observational estimates: The HadCRUT4 data set, *J. Geophys. Res.*, *117*, D08101, doi:10.1029/2011JD017187.

Parker, D., C. Folland, A. Scaife, J. Knight, A. Colman, P. Baines, and B. Dong (2007), Decadal to multidecadal variability and the climate change background, *J. Geophys. Res.*, *112*, D18115, doi:10.1029/2007JD008411.

Pasquini, A. I., and P. J. Depetris (2007), Discharge trends and flow dynamics of South American rivers draining the southern Atlantic seaboard: An overview, *J. Hydrol.*, *333*, 385–399, doi:10.1016/j.jhydrol.2006.09.005.

Pui, A., A. Lal, and A. Sharma (2011), How does the Interdecadal Pacific Oscillation affect design floods in Australia?, *Water Resour. Res.*, *47*, W05554, doi:10.1029/2010WR009420.

Rayner, N. A., D. E. Parker, E. B. Horton, C. K. Folland, L. V. Alexander, D. P. Rowell, E. C. Kent, and A. Kaplan (2003), Global analyses of sea surface temperature, sea ice, and night marine air temperature since the late nineteenth century, *J. Geophys. Res.*, *108*, 4407, doi:10.1029/2002JD002670.

Robertson, A. W., and C. R. Mechoso (1998), Interannual and decadal cycles in river flows of southeastern South America, *J. Clim.*, *11*, 2570–2581.

Robertson, A. W., and C. R. Mechoso (2000), Interannual and interdecadal variability of the South Atlantic convergence zone, *Mon. Weather Rev.*, *128*, 2947–2957.

Robertson, A. W., C. R. Mechoso, and N. O. García (2001), Interannual prediction of the Paraná River, *Geophys. Res. Lett.*, *28*, 4235–4238, doi:10.1029/2000GL012197.

Ropelewski, C. F., and P. D. Jones (1987), An extension of the Tahiti-Darwin Southern Oscillation Index, *Mon. Weather Rev.*, *115*, 2161–2165.

Schlotthauer, G., M. E. Torres, and H. L. Rufiner (2009), A new algorithm for instantaneous F0 speech extraction based on ensemble empirical mode decomposition, in *Proc. of the 17th European Signal Processing Conference (EUSIPCO 2009)*, pp. 2347–2351, Glasgow, Scotland.

Schneider, U., A. Becker, P. Finger, A. Meyer-Christoffer, B. Rudolf, and M. Ziese (2011), GPCC full data reanalysis version 6.0 at 0.5°: Monthly land-surface precipitation from rain-gauges built on GTS-based and historic data, doi:10.5676/DWD_GPCC/FD_M_V6_050..

Torres, M. E., M. A. Colominas, G. Schlotthauer, and P. Flandrin (2011), A complete ensemble empirical mode decomposition with adaptive noise, paper presented at 2011 IEEE International Conference on Acoustics, Speech and Signal Processing ICASSP-11, Prague (CZ), pp. 4144–4147, doi:10.1109/ICASSP.2011.5947265..

Trenberth, K. E., et al. (2007), Observations: Surface and atmospheric climate change, in *Climate Change 2007: The Physical Science Basis. Contribution of Working Group I to the Fourth Assessment Report of the Intergovernmental Panel on Climate Change*, edited by S. Solomon et al., pp. 235–336, Cambridge Univ. Press, Cambridge.

Tucci, C. E. M., and R. T. Clarke (1998), Environmental issues in the la Plata Basin, *Int. J. Water Resour. D.*, *14*, 157–173.

Wolter, K., and M. S. Timlin (2011), El Niño/Southern Oscillation behaviour since 1871 as diagnosed in an extended multivariate ENSO index (MEI.ext), *Int. J. Climatol.*, *31*, 1074–1087, doi:10.1002/joc.2336.

Wu, P., N. Christidis, and P. Stott (2013), Anthropogenic impact on Earth's hydrological cycle, *Nature Clim. Change*, *3*, 807–810, doi:10.1038/nclimate1932.

Wu, Z., and N. E. Huang (2009), Ensemble empirical mode decomposition: A noise-assisted data analysis method, *Adv. Adapt. Data. Anal.*, *1*, 1–41, doi:10.1142/S1793536909000047.

Wu, Z., N. E. Huang, S. R. Long, and C.-K. Peng (2007), On the trend, detrending, and variability of nonlinear and nonstationary time series, *Proc. Natl. Acad. Sci.*, *104*, 14,889–14,894, doi:10.1073/pnas.0701020104.

Wu, Z., E. Schneider, B. Kirtman, E. Sarachik, N. Huang, and C. Tucker (2008), The modulated annual cycle: An alternative reference frame for climate anomalies, *Clim. Dyn.*, *31*, 823–841, doi:10.1007/s00382-008-0437-z.

Wu, Z., N. E. Huang, J. M. Wallace, B. V. Smoliak, and X. Chen (2011), On the time-varying trend in global-mean surface temperature, *Clim. Dyn.*, *37*, 759–773, doi:10.1007/s00382-011-1128-8.